PROCEEDINGS OF THE ROYAL SOCIETY A

rspa.royalsocietypublishing.org

Research

Cite this article: Rudykh S, Bhattacharya K, deBotton G. 2014 Multiscale instabilities in soft heterogeneous dielectric elastomers. *Proc. R. Soc. A* **470**: 20130618.
http://dx.doi.org/10.1098/rspa.2013.0618

Received: 17 September 2013
Accepted: 20 November 2013

Subject Areas:
mechanics

Keywords:
electroactive polymer, dielectric elastomer, composites, electroactive, instability, microstructure

Author for correspondence:
S. Rudykh
e-mail: rudykh@mit.edu

Multiscale instabilities in soft heterogeneous dielectric elastomers

S. Rudykh[1], K. Bhattacharya[2] and G. deBotton[3]

[1]Department of Mechanical Engineering, Massachusetts Institute of Technology, Cambridge, MA, USA
[2]Division of Engineering and Applied Science, California Institute of Technology, Pasadena, CA, USA
[3]Department of Mechanical Engineering, Ben-Gurion University, Beer-Sheva 84105, Israel

The development of instabilities in soft heterogeneous dielectric elastomers is investigated. Motivated by experiments and possible applications, we use in our analysis the physically relevant referential electric field instead of electric displacement. In terms of this variable, a closed form solution is derived for the class of layered neo-Hookean dielectrics. A criterion for the onset of electromechanical multiscale instabilities for the layered composites with *anisotropic* phases is formulated. A *general* condition for the onset of the macroscopic instability in soft multiphase dielectrics is introduced. In the example of the layered dielectrics, the essential influence of the microstructure on the onset of instabilities is revealed. We found that: (i) *macroscopic* instabilities dominate at moderate volume fractions of the stiffer phase, (ii) *interface* instabilities appear at small volume fractions of the stiffer phase and (iii) instabilities of a *finite* scale, comparable to the microstructure size, occur at large volume fractions of the stiffer phase. The latest new type of instabilities does not appear in the purely mechanical case and dominates in the region of large volume fractions of the stiff phase.

1. Introduction

Dielectric elastomers (DEs) respond to external electric stimuli by changing their size and shape. These soft dielectrics can be used to convert electrical energy into mechanical work. As promising actuators, DEs offer the benefits of light weight, fast response and simple principles of work. The field of DEs has been

intensively studied experimentally and theoretically in the last decade, and, consequently, nowadays these actuators are feasible [1–12]. In spite of the significant progress, these materials are limited by the extremely large electric fields that they require for meaningful actuation. The reason for this is the poor electromechanical coupling in typical polymers which have a limited ratio of dielectric to elastic modulus. An approach to challenge the issue is to consider *heterogeneous* DEs by combining an elastomer with a high dielectric or even conductive material [13–17]. This approach has been shown to be promising in experiments [8,18]. Moreover, theoretical estimations [19–21] show that the experimental results are only a beginning, and proper optimization of the microstructure can lead to orders of magnitude improvement in electromechanical coupling.

For example, a heterogeneous DE characterized by (i) soft mode of deformation and (ii) amplification of the local electric field by active inclusions was recently proposed by Rudykh *et al.* [21]. In these heterogeneous DEs, the material deforms in the soft mode of deformation owing to an appropriately applied external electric field. The perspectives of these heterogeneous DEs depend on the advances in the multi-material three-dimensional printing and other techniques, which already allow manufacturing of layered materials with varying dielectric properties and layer thicknesses comparable to visible light wavelength and even subwavelength size [22].

An intriguing possibility that has emerged in recent years is the exploitation of instabilities associated with finite deformation for enhancing the actuation. Specifically, Mockensturm & Goulbourne [23] and Rudykh *et al.* [24] showed that the aneurism instabilities in balloons can lead to dramatically enhanced electromechanical coupling. Moreover, the instability-induced microstructure transformations in layered media [25] can be used for designing materials with switchable properties, e.g. wave propagation can be manipulated [26]. A combination of this idea with electromechanical instabilities opens a new avenue for designing switchable phononic and photonic crystals controllable by electric field. These ideas motivate this work.

While purely mechanical instabilities have been studied intensively for decades [25,27–32], relatively less is known about coupled instabilities. Much of the existing work on coupled instabilities is motivated by failure. Examples include the study of pull-in instabilities [33,34], electrical breakdown [8,35] and failure mechanisms at high electric fields [36] in homogeneous media as well as electrical breakdown of DE with random distribution of the inclusions [37,38].

Dorfmann & Ogden [39] wrote the incremental equations of electro-elasto-statics about a finite deformation, and used it to study the stability of homogeneous half-space. Rudykh & deBotton [40] and Rudykh & Bertoldi [41] have studied macroscopic instabilities of general anisotropic media. Recently, Bertoldi & Gei [42] investigated instabilities in soft-layered dielectrics with isotropic phases in which the electric field is perpendicular to the layers and an uniaxial prestretch is applied along the layers. They showed the presence of various instabilities including microscopic (short wavelength) instability, macroscopic instability (loss of ellipticity of the effective media) and the loss of positive definiteness of the tangent operator.

In this work, we revisit the problem of coupled electromechanical instabilities in layered media and study material instabilities. We formulate the problem in terms of electrostatic potential as the primary field variable, as opposed to the electric displacement which is used in previous works [40–42]. While the use of electric displacement leads to a simpler mathematical problem, it is not natural from an experimental viewpoint. In experimental practice, it is significantly simpler to prescribe the electrostatic potential on a surface than to prescribe the exact charge distribution. Further, the study of electrical breakdown is direct because breakdown criteria are prescribed in terms of the electric field. Furthermore, as we shall see, it is simpler to predict the onset of instabilities in this setting. All of this makes it simpler to identify critical microstructures. The second point of departure from previous work is that we formulate the equations for anisotropic media. This is important as the effective microstructures resulting in large coupling [20,21] also give rise to anisotropy at the macroscopic level. Finally, we consider a more general setting where

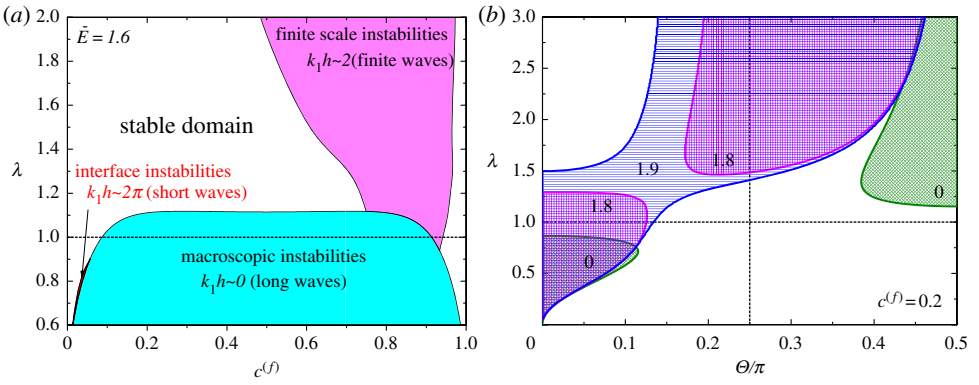

Figure 1. The unstable domains of layered soft dielectric subjected to an electric excitation and prestretch λ. Different types of instabilities and their domains are presented as functions of the volume fraction of the stiff phase $c^{(f)}$ (*a*) and the direction of anisotropy Θ (*b*). (Online version in colour.)

the electric field and mechanical loading are applied at an arbitrary angle to the layers. Again, this is motivated by considerations of enhanced actuation [20,21].

Figure 1 summarizes the main result of the study. We find three modes of instability depending on the geometry and applied loads: a *macroscopic instability* characterized by long wavelengths (or loss of ellipticity of the homogenized response), a *microscopic instability* characterized by short wavelengths, and an *interface instability* also characterized by short wavelengths that occur in materials with dilute concentration of the stiffer phase. In the last instability, the perturbations are limited to a narrow layer of the soft material, and thus share features with instabilities associated with a thin stiff layer supported on an infinite compliant material.

Figure 1*a* is a 'phase diagram' of the stable and unstable regions in the space of applied stretch along the layers and volume fraction. The electric field is held fixed at a moderate value normal to the layers. The interface instability occurs (as expected) at dilute concentrations of the stiff phase under compressive stretch, and is suppressed by a large electric field. Thus, this instability is the remnant of the instability that occurs in the purely mechanical setting [29]. The macroscopic instability occurs at moderate volume fractions of the stiff phase and under compressive or limited tensile stretch, and the unstable region increases with electric field. This instability is again largely mechanical: the imposed compressive or limited tensile stretch introduces a compressive stress as the material seeks to elongate owing to the applied electric field. The microscopic instability occurs at large volume fractions of the stiff high dielectric phase and is a result of electro-mechanical interaction. The high contrast in dielectric moduli implies that the electric field is inversely proportional to the volume fraction of the compliant phase. Thus, as the volume fraction of the stiff phase increases, the electric field and the electrostatically induced stress increase in the compliant phase. This stress is relieved by the instability that allows for the alternating compliant layers to locally expand while only bending the stiff layers. These are consistent with the findings of Bertoldi & Gei [42].

Figure 1*b* shows how these results change as we change the angle between the layers and the applied stretch. The electric field is still perpendicular to the applied stretch (and consequently inclined to the layers). Specifically, we focus on the macroscopic instability, and thus focus on a volume fraction of 0.2 for the stiff material. For small and intermediate electric fields (0–1.8), macroscopic instabilities occur at small angles (at small stretch) as well as for large angles (at high stretch), and there are no macroscopic instabilities at intermediate angles. This is because at intermediate angles the layers can rotate to avoid instability. We recall that layer rotation is also a mechanism for large actuation [20,21]. This region of stability closes at sufficiently high electric fields.

2. Theoretical background

(a) Formulation

The Cartesian position vector of a material point in a reference configuration of a body is $\mathbf{X}$ and its position vector in the deformed configuration is $\mathbf{x}$. The deformation of the body is characterized by the mapping $\mathbf{x}=\boldsymbol{\chi}(\mathbf{X})$. The deformation gradient is $\mathbf{F}=\partial\boldsymbol{\chi}(\mathbf{X})/\partial\mathbf{X}$. The ratio between the volumes in the deformed and undeformed states is $J\equiv\det\mathbf{F}$.

We assume that the deformation is quasi-static, no magnetic field is present, and no charge is present in the dielectric. Consequently, Maxwell equations reduce to

$$\operatorname{div}\mathbf{D}=0\quad\text{and}\quad\operatorname{curl}\mathbf{E}=0, \tag{2.1}$$

where $\mathbf{D}$ is the electric displacement and $\mathbf{E}$ is the electric field. We distinguish between the differential operators div(•), curl(•) and grad(•) in the current configuration and the operators Div(•), Curl(•) and Grad(•) in the reference configuration. Equations (2.1) can be rewritten in terms of the referential electric field $\mathbf{E}^0=\mathbf{F}^{\mathrm{T}}\mathbf{E}$ and the referential electric displacement $\mathbf{D}^0=J\mathbf{F}^{-1}\mathbf{D}$ [39,43] as

$$\operatorname{Div}\mathbf{D}^0=0\quad\text{and}\quad\operatorname{Curl}\mathbf{E}^0=0. \tag{2.2}$$

In this work, we follow the notation proposed recently by Dorfmann & Ogden [39,43] and consider elastic dielectrics whose constitutive relation is given in terms of a scalar-valued energy-density function $\Psi(\mathbf{F},\mathbf{E}^0)$ such that

$$\mathbf{P}=\frac{\partial\Psi(\mathbf{F},\mathbf{E}^0)}{\partial\mathbf{F}}\quad\text{and}\quad\mathbf{D}^0=-\frac{\partial\Psi(\mathbf{F},\mathbf{E}^0)}{\partial\mathbf{E}^0}, \tag{2.3}$$

where $\mathbf{P}$ is the *total* nominal stress tensor. The corresponding true or Cauchy total stress tensor is related to the nominal stress tensor via the relation $\boldsymbol{\sigma}=J^{-1}\mathbf{P}\mathbf{F}^{\mathrm{T}}$. For an incompressible material, the nominal stress tensor is

$$\mathbf{P}=\frac{\partial\Psi(\mathbf{F},\mathbf{E}^0)}{\partial\mathbf{F}}-p\mathbf{F}^{-\mathrm{T}}, \tag{2.4}$$

where p is an arbitrary pressure-like scalar. In the absence of body forces, the equilibrium equations are

$$\operatorname{Div}\mathbf{P}=0. \tag{2.5}$$

The incremental governing equations [39] are

$$\operatorname{Div}\dot{\mathbf{P}}=0,\quad\operatorname{Div}\dot{\mathbf{D}}^0=0\quad\text{and}\quad\operatorname{Curl}\dot{\mathbf{E}}^0=0. \tag{2.6}$$

where $\dot{\mathbf{P}}$, $\dot{\mathbf{D}}^0$ and $\dot{\mathbf{E}}^0$ are infinitesimal changes in the nominal stress, electric displacement and electrical field, respectively. The linearized constitutive equations are provided via the electroelastic moduli tensors

$$\mathcal{A}^0_{i\alpha k\beta}=\frac{\partial^2\Psi}{\partial F_{i\alpha}\partial F_{k\beta}},\quad\mathcal{G}^0_{i\alpha\beta}=\frac{\partial^2\Psi}{\partial F_{i\alpha}\partial E^0_{\beta}}\quad\text{and}\quad\mathcal{E}^0_{\alpha\beta}=\frac{\partial^2\Psi}{\partial E^0_{\alpha}\partial E^0_{\beta}}, \tag{2.7}$$

namely,

$$\dot{P}_{ij}=\mathcal{A}^0_{ijkl}\dot{F}_{kl}+\mathcal{G}^0_{ijk}\dot{E}^0_k\quad\text{and}\quad-\dot{D}^0_i=\mathcal{G}^0_{jki}\dot{F}_{jk}+\mathcal{E}^0_{ij}\dot{E}^0_j. \tag{2.8}$$

For an incompressible material, the linearized constitutive relations are

$$\dot{P}_{ij}=\mathcal{A}^0_{ijkl}\dot{F}_{kl}+\mathcal{G}^0_{ijk}\dot{E}^0_k-\dot{p}F^{-\mathrm{T}}_{ij}+pF^{-1}_{jk}\dot{F}_{kl}F^{-1}_{li},\quad-\dot{D}^0_i=\mathcal{G}^0_{jki}\dot{F}_{jk}+\mathcal{E}^0_{ij}\dot{E}^0_j, \tag{2.9}$$

where $\dot{p}$ is an incremental change in pressure.

Consider the current configuration as a new reference configuration. We recall that $\dot{\mathbf{F}}=(\operatorname{grad}\mathbf{v})\mathbf{F}$, where $v_i=\dot{x}_i$ is an incremental displacement. The incremental 'push-forward' of $\dot{\mathbf{P}}$, $\dot{\mathbf{E}}^0$

and $\dot{\mathbf{D}}^0$ to the current configuration are

$$\dot{\mathbf{T}} = J^{-1}\dot{\mathbf{P}}\mathbf{F}^{\mathrm{T}}, \quad \dot{\mathbf{D}} = J^{-1}\mathbf{F}\dot{\mathbf{D}}^0 \quad \text{and} \quad \dot{\mathbf{E}} = \mathbf{F}^{-\mathrm{T}}\dot{\mathbf{E}}^0. \tag{2.10}$$

In terms of these increments, the linearized constitutive equations are

$$\dot{T}_{ij} = \mathcal{A}_{ijkl}v_{k,l} + \mathcal{G}_{ijk}\dot{E}_k - \dot{p}\delta_{ij} + pv_{j,i}, \quad -\dot{D}_i = \mathcal{G}_{jki}v_{j,k} + \mathcal{E}_{ij}\dot{E}_j, \tag{2.11}$$

where

$$\mathcal{A}_{ijkl} = J^{-1}F_{j\alpha}F_{l\beta}\mathcal{A}^0_{i\alpha k\beta}, \quad \mathcal{G}_{ijk} = J^{-1}F_{j\alpha}F_{k\beta}\mathcal{G}^0_{i\alpha\beta} \quad \text{and} \quad \mathcal{E}_{ij} = J^{-1}F_{i\alpha}F_{j\beta}\mathcal{E}^0_{\alpha\beta}. \tag{2.12}$$

The electroelastic moduli possess the symmetries

$$\mathcal{A}_{ijkl} = \mathcal{A}_{klij}, \quad \mathcal{G}_{ijk} = \mathcal{G}_{jik} \quad \text{and} \quad \mathcal{E}_{ij} = \mathcal{E}_{ji}. \tag{2.13}$$

Incremental governing equations (2.6) become

$$\operatorname{div}\dot{\mathbf{T}} = 0, \quad \operatorname{div}\dot{\mathbf{D}} = 0 \quad \text{and} \quad \operatorname{curl}\dot{\mathbf{E}} = 0. \tag{2.14}$$

Upon substitution of linearized relations (2.11) in $(2.14)_1$ and $(2.14)_2$, the following equations are obtained

$$\mathcal{A}_{ijkl}v_{k,lj} + \mathcal{G}_{ijk}\dot{E}_{k,j} - \dot{p}_{,i} = 0 \quad \text{and} \quad \mathcal{G}_{jki}v_{j,ki} + \mathcal{E}_{ij}\dot{E}_{j,i} = 0. \tag{2.15}$$

The instability is associated with the existence of a non-trivial solution to these equations (2.15).

(b) Macroscopic instabilities

We begin by what are termed macroscopic instabilities in the literature. In a homogeneous material, they correspond to the instability of a homogeneous state. In a heterogeneous periodic material, they correspond to instabilities of infinite extent compared to the unit cell. In this situation, we replace the periodic material with a homogeneous material with homogenized properties. So, we assume in this section that the incremental moduli $\mathcal{A}_{ijkl}$, $\mathcal{G}_{ijk}$ and $\mathcal{E}_{ij}$ are uniform.

We seek a solution to (2.15) of the form

$$v_i = \tilde{v}_i f(\hat{\mathbf{a}}\cdot\mathbf{x}), \quad \dot{p} = \tilde{q}f'(\hat{\mathbf{a}}\cdot\mathbf{x}) \quad \text{and} \quad \dot{E}_i = \tilde{e}_i f'(\hat{\mathbf{a}}\cdot\mathbf{x}), \tag{2.16}$$

where f is a continuous and sufficiently differentiable function, $\hat{\mathbf{a}} = a_1\bar{\mathbf{e}}_1 + a_2\bar{\mathbf{e}}_2 + a_3\bar{\mathbf{e}}_3$ is a unit vector; $\tilde{v}_i$, $\tilde{e}_i$ and $\tilde{q}$ are incremental macroscopic quantities independent of $\mathbf{x}$. The incompressibility constraint together with the last of (2.14) provide additional equations for $\tilde{v}_i$ and $\tilde{e}_i$. In particular, for a plane problem

$$\tilde{v}_1 = -\xi\tilde{v}_2 \quad \text{and} \quad \tilde{e}_1 = \xi^{-1}\tilde{e}_2, \tag{2.17}$$

where $\xi \equiv a_2/a_1$. Upon substitution of expressions (2.16) together with (2.17) into (2.15), elimination of the pressure increment leads to a polynomial equation in ξ, namely

$$\Gamma_6\xi^6 + \Gamma_5\xi^5 + \Gamma_4\xi^4 + \Gamma_3\xi^3 + \Gamma_2\xi^2 + \Gamma_1\xi + \Gamma_0 = 0, \tag{2.18}$$

where the coefficients Γ_i are given by the electroelastic moduli as follows:

$$\Gamma_0 = \mathcal{G}_{121}^2 - \mathcal{A}_{2121}\mathcal{E}_{11}, \quad \Gamma_1 = 2(-\mathcal{A}_{2121}\mathcal{E}_{12} + (\mathcal{A}_{1121} - \mathcal{A}_{2122})\mathcal{E}_{11} + \mathcal{G}_{121}(\mathcal{G}_{221} + \mathcal{G}_{122} - \mathcal{G}_{111})),$$

$$\Gamma_2 = -\mathcal{A}_{2121}\mathcal{E}_{22} + 4(\mathcal{A}_{1121} - \mathcal{A}_{2122})\mathcal{E}_{12} - (\mathcal{A}_{1111} - 2\mathcal{A}_{1122} - 2\mathcal{A}_{1221} + \mathcal{A}_{2222})\mathcal{E}_{11} - 2\mathcal{G}_{121}(\mathcal{G}_{112} + \mathcal{G}_{121} - \mathcal{G}_{222}) + (\mathcal{G}_{122} + \mathcal{G}_{221} - \mathcal{G}_{111})^2,$$

$$\Gamma_3 = -2((\mathcal{A}_{1112} - \mathcal{A}_{1222})\mathcal{E}_{11} + (\mathcal{A}_{1111} - 2\mathcal{A}_{1122} - 2\mathcal{A}_{1221} + \mathcal{A}_{2222})\mathcal{E}_{12} + (\mathcal{A}_{2122} - \mathcal{A}_{1121})\mathcal{E}_{22} + (\mathcal{G}_{121}\mathcal{G}_{122} - (\mathcal{G}_{111} - \mathcal{G}_{122} - \mathcal{G}_{221})(\mathcal{G}_{112} + \mathcal{G}_{121} - \mathcal{G}_{222}))),$$

$$\Gamma_4 = -(\mathcal{A}_{1111} - 2\mathcal{A}_{1122} - 2\mathcal{A}_{1221} + \mathcal{A}_{2222})\mathcal{E}_{22} - 4(\mathcal{A}_{1112} - \mathcal{A}_{1222})\mathcal{E}_{12} - \mathcal{A}_{1212}\mathcal{E}_{11} + (\mathcal{G}_{112} + \mathcal{G}_{121} - \mathcal{G}_{222})^2 + 2\mathcal{G}_{122}(\mathcal{G}_{111} - \mathcal{G}_{122} - \mathcal{G}_{221}),$$

$$\Gamma_5 = 2((\mathcal{A}_{1222} - \mathcal{A}_{1112})\mathcal{E}_{22} - \mathcal{A}_{1212}\mathcal{E}_{12} + \mathcal{G}_{122}(\mathcal{G}_{112} + \mathcal{G}_{121} - \mathcal{G}_{222})) \quad \text{and}$$

$$\Gamma_6 = \mathcal{G}_{122}^2 - \mathcal{A}_{1212}\mathcal{E}_{22}.$$

A macroscopic instability is associated with a real solution to (2.18). We once again note that condition (2.18) can be used for the macroscopic instability analysis of *multiphase* hyperelastic dielectrics. Once the macroscopic electroelastic moduli are determined either via a homogenization technique or numerically (for the purely mechanical case [32]), the stable domains can be deduced from (2.18) for any microstructure and any planar mechanical and electrical loadings.

Heterogeneous periodic materials may also suffer from microscopic instabilities. These become too difficult to explicitly analyse for arbitrary microstructures. Therefore, we examine to the case of layered materials.

(c) Layered materials

Consider a layered dielectric composite made out of two incompressible phases with volume fractions $c^{(m)}$ and $c^{(f)} = 1 - c^{(m)}$. Here and thereafter, the fields and parameters of the stiff and the soft phases are denoted by superscripts $(\bullet)^{(f)}$ and $(\bullet)^{(m)}$, respectively. Geometrically, the layers are characterized by their thicknesses $h^{(m)} = hc^{(m)}$ and $h^{(f)} = hc^{(f)}$, where $h = h^{(m)} + h^{(f)}$ is the thickness of the repeated unit cell (figure 2). The direction normal to the layers plane is the laminate direction $\hat{\mathbf{N}}$, and $\hat{\mathbf{M}}$ is a unit vector tangent to the interface, both in the undeformed configuration (figure 2). Assuming that along the primary branch of the solution all the fields are homogeneous in each phase, we have that the mean nominal electric field in the composite is

$$\bar{\mathbf{E}}^0 = c^{(m)}\mathbf{E}^{0(m)} + c^{(f)}\mathbf{E}^{0(f)}. \tag{2.19}$$

The continuity condition on the electric field is

$$(\mathbf{E}^{0(m)} - \mathbf{E}^{0(f)}) \cdot \hat{\mathbf{M}} = 0 \quad \text{or} \quad \mathbf{E}^{0(m)} - \mathbf{E}^{0(f)} = \beta\hat{\mathbf{N}}, \tag{2.20}$$

where β is a scalar. Accordingly, the referential electric field in each phase can be expressed in the form

$$\mathbf{E}^{0(m)} = \bar{\mathbf{E}}^0 + c^{(f)}\beta\hat{\mathbf{N}} \quad \text{and} \quad \mathbf{E}^{0(f)} = \bar{\mathbf{E}}^0 - c^{(m)}\beta\hat{\mathbf{N}}. \tag{2.21}$$

As the interface is charge free, the continuity condition on the referential electric displacement field is

$$(\mathbf{D}^{0(m)} - \mathbf{D}^{0(f)}) \cdot \hat{\mathbf{N}} = 0. \tag{2.22}$$

For incompressible laminates the displacement continuity condition [44] leads to

$$\mathbf{F}^{(m)} = \bar{\mathbf{F}}(\mathbf{I} + c^{(f)}\alpha\hat{\mathbf{M}} \otimes \hat{\mathbf{N}}) \quad \text{and} \quad \mathbf{F}^{(f)} = \bar{\mathbf{F}}(\mathbf{I} - c^{(m)}\alpha\hat{\mathbf{M}} \otimes \hat{\mathbf{N}}), \tag{2.23}$$

where α is a constant. The corresponding interface stress continuity condition [19] is

$$(\mathbf{P}^{(m)} - \mathbf{P}^{(f)}) \cdot \hat{\mathbf{N}} = 0. \tag{2.24}$$

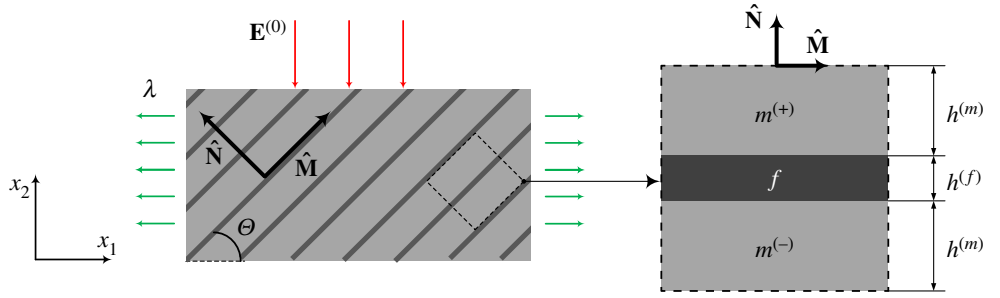

Figure 2. Electroactive layered composite subjected to electric excitation. (Online version in colour.)

Once the constitutive relations for phases are prescribed, the constants α and β can be determined from continuity conditions (2.22) and (2.24). This completes the solution up to a bifurcation point.

(d) Microscopic instability in layered materials

To determine the onset of instabilities in the composites an analysis similar to that used in [29,42] is adopted. In each phase, we seek a solution of (2.15) in the form

$$v_i = \tilde{v}_i(x_2)\exp(\mathrm{i}k_1x_1), \quad \dot{p} = \tilde{q}(x_2)\exp(\mathrm{i}k_1x_1) \quad \text{and} \quad \dot{E}_i = \tilde{e}_i(x_2)\exp(\mathrm{i}k_1x_1), \tag{2.25}$$

where k_1 is the wave number along the x_1-direction (figure 2). The incompressibility constraint together with the absence of the electric field vorticity provide two equations for $\tilde{v}_i$ and $\tilde{e}_i$

$$\tilde{v}_2' = -\mathrm{i}k_1\tilde{v}_1 \quad \text{and} \quad \tilde{e}_1' = \mathrm{i}k_1\tilde{e}_2, \tag{2.26}$$

where the notation $(\bullet)' = (\bullet)_{,2}$ is introduced. The resulting incremental governing equations (2.15) read

$$\begin{aligned} &k_1^2(\mathcal{A}_{1122}+\mathcal{A}_{1221}-\mathcal{A}_{1111})\tilde{v}_1 + \mathrm{i}k_1(2\mathcal{A}_{1112}-\mathcal{A}_{1222})\tilde{v}_1' + \mathcal{A}_{1212}\tilde{v}_1'' - k_1^2\mathcal{A}_{1121}\tilde{v}_2 \\ &\quad + \mathrm{i}k_1\mathcal{G}_{111}\tilde{e}_1 + \mathrm{i}k_1(\mathcal{G}_{112}+\mathcal{G}_{121})\tilde{e}_2 + \mathcal{G}_{122}\tilde{e}_2' - \mathrm{i}k_1\tilde{q} = 0, \end{aligned} \tag{2.27}$$

$$\begin{aligned} &k_1^2(2\mathcal{A}_{2122}-\mathcal{A}_{1121})\tilde{v}_1 + \mathrm{i}k_1(\mathcal{A}_{1221}+\mathcal{A}_{1122}-\mathcal{A}_{2222})\tilde{v}_1' + \mathcal{A}_{1222}\tilde{v}_1'' - k_1^2\mathcal{A}_{2121}\tilde{v}_2 \\ &\quad + \mathrm{i}k_1\mathcal{G}_{121}\tilde{e}_1 + \mathrm{i}k_1(\mathcal{G}_{122}+\mathcal{G}_{221})\tilde{e}_2 + \mathcal{G}_{222}\tilde{e}_2' - \tilde{q}' = 0 \end{aligned} \tag{2.28}$$

and

$$\begin{aligned} &k_1^2(\mathcal{G}_{122}+\mathcal{G}_{221}-\mathcal{G}_{111})\tilde{v}_1 + \mathrm{i}k_1(\mathcal{G}_{112}+\mathcal{G}_{121}-\mathcal{G}_{222})\tilde{v}_1' + \mathcal{G}_{122}\tilde{v}_1'' - k_1^2\mathcal{G}_{121}\tilde{v}_2 \\ &\quad + \mathrm{i}k_1\mathcal{E}_{11}\tilde{e}_1 + 2\mathrm{i}k_1\mathcal{E}_{12}\tilde{e}_2 + \mathcal{E}_{22}\tilde{e}_2' = 0. \end{aligned} \tag{2.29}$$

Equations (2.26)–(2.29) provide a set of six linear homogeneous first-order differential equations that depend on the vector of six unknowns $\tilde{\mathbf{u}} = (\tilde{v}_1, \tilde{v}_2, \tilde{e}_1, \tilde{e}_2, \tilde{q}, \tilde{v}_1')$

$$\mathbf{R}\tilde{\mathbf{u}} = \tilde{\mathbf{u}}'. \tag{2.30}$$

The components of the matrix $\mathbf{R}$ are given in appendix A. The solution of the system can be determined in the form

$$\tilde{\mathbf{u}} = \mathbf{BZs}, \tag{2.31}$$

where $\mathbf{s}$ is an arbitrary constant vector that will be determined later from the continuity and quasi-periodicity conditions on the unit cell. In (2.31), $\mathbf{Z}(x_2) = \mathrm{diag}[\exp(\mathbf{z}x_2)]$ is the diagonal matrix of the eigenvalues vector $\mathbf{z}$ of the matrix $\mathbf{R}$, and the corresponding eigenvectors of $\mathbf{R}$ are the columns of the matrix $\mathbf{B}$.

Consider the periodic unit cell of the layered composite shown in figure 2. The quasi-periodic boundary conditions are

$$\tilde{\mathbf{u}}(x_2+h)=\tilde{\mathbf{u}}(x_2)\exp(\mathrm{i}k_2h), \tag{2.32}$$

where $k_2\in[0,2\pi/h)$ is the solution periodicity parameter, also referred to as Floquet parameter. In the interval $0<x_2<h+h^{(m)}$, solution (2.31) attains the form

$$\left.\begin{aligned}\tilde{\mathbf{u}}(x_2)&=\overset{m}{\mathbf{B}}\overset{m}{\mathbf{Z}}(x_2)\overset{m-}{\mathbf{s}}, \quad 0<x_2<h^{(m)},\\ \tilde{\mathbf{u}}(x_2)&=\overset{f}{\mathbf{B}}\overset{f}{\mathbf{Z}}(x_2)\overset{f}{\mathbf{s}}, \quad h^{(m)}<x_2<h\\ \text{and}\quad \tilde{\mathbf{u}}(x_2)&=\overset{m}{\mathbf{B}}\overset{m}{\mathbf{Z}}(x_2)\overset{m+}{\mathbf{s}}, \quad h<x_2<h+h^{(m)},\end{aligned}\right\} \tag{2.33}$$

where $\overset{m}{\mathbf{z}}$, $\overset{f}{\mathbf{z}}$ are the eigenvalues of $\mathbf{R}$ in which the electroelastic moduli correspond to the appropriate phase, $\overset{m}{\mathbf{B}}$ and $\overset{f}{\mathbf{B}}$ are the corresponding matrices of eigenvectors. Substitution of (2.33) into (2.32) yields

$$\overset{m+}{\mathbf{s}}=\exp(\mathrm{i}k_2h)(\overset{m}{\mathbf{Z}}(h))^{-1}\overset{m-}{\mathbf{s}}. \tag{2.34}$$

The jump conditions of the incremental fields at the interfaces are

$$[\![v]\!]=0, \quad [\![\dot{\mathbf{T}}]\!]\mathbf{n}=\mathbf{0}, \quad [\![\dot{\mathbf{D}}]\!]\cdot\mathbf{n}=0 \quad \text{and} \quad \mathbf{n}\times[\![\dot{\mathbf{E}}]\!]=0, \tag{2.35}$$

where $\mathbf{n}=\mathbf{F}^{-\mathrm{T}}\hat{\mathbf{N}}$ is normal to the interface at the current configuration, and the notation $[\![\bullet]\!]\equiv(\bullet)^+-(\bullet)^-$ is used. By making use of (2.25) and (2.26), the jump conditions (2.35) are

$$[\![\tilde{v}_1]\!]=0, \quad [\![\tilde{v}_2]\!]=0 \quad \text{and} \quad [\![\tilde{e}_1]\!]n_2-[\![\tilde{e}_2]\!]n_1=0, \tag{2.36}$$

$$\begin{aligned}&[\![\mathrm{i}k_1(\mathcal{A}_{1111}-\mathcal{A}_{1122}+p)\tilde{v}_1+\mathcal{A}_{1112}\tilde{v}_1'+\mathrm{i}k_1\mathcal{A}_{1121}\tilde{v}_2+\mathcal{G}_{111}\tilde{e}_1+\mathcal{G}_{112}\tilde{e}_2-\tilde{q}]\!]n_1\\&\quad+[\![\mathrm{i}k_1(\mathcal{A}_{1211}-\mathcal{A}_{1222})\tilde{v}_1+\mathcal{A}_{1212}\tilde{v}_1'+\mathrm{i}k_1(\mathcal{A}_{1221}+p)\tilde{v}_2+\mathcal{G}_{121}\tilde{e}_1+\mathcal{G}_{122}\tilde{e}_2]\!]n_2=0,\end{aligned} \tag{2.37}$$

$$\begin{aligned}&[\![\mathrm{i}k_1(\mathcal{A}_{2111}-\mathcal{A}_{2122})\tilde{v}_1+(\mathcal{A}_{2112}+p)\tilde{v}_1'+\mathrm{i}k_1\mathcal{A}_{2121}\tilde{v}_2+\mathcal{G}_{211}\tilde{e}_1+\mathcal{G}_{212}\tilde{e}_2]\!]n_1\\&\quad+[\![\mathrm{i}k_1(\mathcal{A}_{2211}-\mathcal{A}_{2222}-p)\tilde{v}_1+\mathcal{A}_{2212}\tilde{v}_1'+\mathrm{i}k_1\mathcal{A}_{2221}\tilde{v}_2+\mathcal{G}_{221}\tilde{e}_1+\mathcal{G}_{222}\tilde{e}_2-\tilde{q}]\!]n_2=0\end{aligned} \tag{2.38}$$

and

$$\begin{aligned}&[\![\mathrm{i}k_1(\mathcal{G}_{111}-\mathcal{G}_{221})\tilde{v}_1+\mathcal{G}_{121}\tilde{v}_1'+\mathrm{i}k_1\mathcal{G}_{211}\tilde{v}_2+\mathcal{E}_{11}\tilde{e}_1+\mathcal{E}_{12}\tilde{e}_2]\!]n_1\\&\quad+[\![\mathrm{i}k_1(\mathcal{G}_{112}-\mathcal{G}_{222})\tilde{v}_1+\mathcal{G}_{122}\tilde{v}_1'+\mathrm{i}k_1\mathcal{G}_{212}\tilde{v}_2+\mathcal{E}_{12}\tilde{e}_1+\mathcal{E}_{22}\tilde{e}_2]\!]n_2=0.\end{aligned} \tag{2.39}$$

Equations (2.36)–(2.39) can be written in the form $[\![\mathbf{Q}\tilde{\mathbf{u}}]\!]=0$. The non-zero entries of the matrix $\mathbf{Q}$ are

$$\begin{aligned}&Q_{11}=Q_{22}=1, \quad Q_{33}=-Q_{34}=n_2, \quad Q_{41}=\mathrm{i}k_1((\mathcal{A}_{1111}-\mathcal{A}_{1122}+p)n_1\\&\qquad+(\mathcal{A}_{1211}-\mathcal{A}_{1222})n_2)\\&Q_{42}=\mathrm{i}k_1(\mathcal{A}_{1121}n_1+(\mathcal{A}_{1211}+p)n_2), \quad Q_{43}=\mathcal{G}_{111}n_1+\mathcal{G}_{121}n_2, \quad Q_{44}=\mathcal{G}_{112}n_1+\mathcal{G}_{122}n_2,\\&Q_{45}=-n_1, \quad Q_{46}=\mathcal{A}_{1112}n_1+\mathcal{A}_{1212}n_2, \quad Q_{51}=\mathrm{i}k_1((\mathcal{A}_{2111}-\mathcal{A}_{2122})n_1\\&\qquad+(\mathcal{A}_{2211}-\mathcal{A}_{2222}-p)n_2),\\&Q_{52}=\mathrm{i}k_1(\mathcal{A}_{2121}n_1+\mathcal{A}_{2221}n_2), \quad Q_{53}=\mathcal{G}_{211}n_1+\mathcal{G}_{221}n_2, \quad Q_{54}=\mathcal{G}_{212}n_1+\mathcal{G}_{222}n_2,\\&Q_{55}=-n_2, \quad Q_{56}=(\mathcal{A}_{2112}+p)n_1+\mathcal{A}_{2212}n_2, \quad Q_{61}=\mathrm{i}k_1((\mathcal{G}_{111}-\mathcal{G}_{221})n_1\\&\qquad+(\mathcal{G}_{112}-\mathcal{G}_{222})n_2),\\&Q_{62}=\mathrm{i}k_1(\mathcal{G}_{211}n_1+\mathcal{G}_{212}n_2), \quad Q_{63}=\mathcal{E}_{11}n_1+\mathcal{E}_{12}n_2, \quad Q_{64}=\mathcal{E}_{12}n_1+\mathcal{E}_{22}n_2 \quad \text{and}\\&Q_{66}=\mathcal{G}_{121}n_1+\mathcal{G}_{122}n_2.\end{aligned}$$

Finally, upon usage of (2.33), we have that

$$\overset{m}{\mathbf{Q}}\overset{m}{\mathbf{B}}\overset{m}{\mathbf{Z}}(h^{(m)})\overset{m-}{\mathbf{s}}=\overset{f}{\mathbf{Q}}\overset{f}{\mathbf{B}}\overset{f}{\mathbf{Z}}(h^{(m)})\overset{f}{\mathbf{s}} \quad \text{and} \quad \overset{m}{\mathbf{Q}}\overset{m}{\mathbf{B}}\overset{m}{\mathbf{Z}}(h)\overset{m+}{\mathbf{s}}=\overset{f}{\mathbf{Q}}\overset{f}{\mathbf{B}}\overset{f}{\mathbf{Z}}(h)\overset{f}{\mathbf{s}}. \tag{2.40}$$

The combination of (2.34) and (2.40) leads to the condition for the existence of a non-trivial solution

$$\det[(\overset{m\,m}{\mathbf{QB}})^{-1}\overset{f\,f\,f}{\mathbf{QBZ}}(h^{(f)})(\overset{f\,f}{\mathbf{QB}})^{-1}\overset{m\,m\,m}{\mathbf{QBZ}}(h^{(m)}) - \mathbf{I}\exp(\mathrm{i}k_2 h)] = 0. \tag{2.41}$$

When condition (2.41) is satisfied for a combination of mechanical and electrical loads, a solution in the form of equation (2.25) that satisfies equations (2.32) and (2.33) exists, where k_2 represents the scale of the periodicity of the solution. A similar condition was derived for the purely mechanical case [29] and for layered composites with isotropic neo-Hookean phases subjected to a prestretch along the layers and electrical displacement excitation perpendicular to the surface [42].

In the preceding analysis, no assumption regarding the phases behaviors was made and composites with *anisotropic* phases can be analysed by following this derivation. Moreover, the derived condition can be used for any planar combination of mechanical and electrical loads and it is not restricted to the aligned prestretch and perpendicular electric excitation assumed in [42].

(e) Macroscopic instability in layered composites

Finally, we specialize the results of §2*b* on macroscopic instabilities to layered materials. We recall that Geymonat *et al.* [45] rigorously showed in the purely mechanical case that the macroscopic instabilities onset corresponds to the existence of a non-trivial solution in the long-wave limit $k_1 h \to 0$. In the context of the coupled problem, Bertoldi & Gei [42] demonstrated that the macroscopic instability analysis agrees with the onset of long-wave instabilities in layered composites with isotropic neo-Hookean phases subjected to a prestretch along the layers and electrical displacement excitation perpendicular to the layers.

As the basic solution to layered materials is piecewise constant, the energy-density function of the composite can be expressed as the weighted sum of the phase energy-density functions

$$\tilde{\Psi}(\bar{\mathbf{F}}, \bar{\mathbf{E}}^0) = c^{(m)}\Psi^{(m)}(\bar{\mathbf{F}}, \bar{\mathbf{E}}^0) + c^{(f)}\Psi^{(f)}(\bar{\mathbf{F}}, \bar{\mathbf{E}}^0). \tag{2.42}$$

The average nominal stress tensor and electric displacement are

$$\bar{\mathbf{P}} = \frac{\partial \tilde{\Psi}}{\partial \bar{\mathbf{F}}} - p\bar{\mathbf{F}}^{-\mathrm{T}} \quad \text{and} \quad \bar{\mathbf{D}}^0 = -\frac{\partial \tilde{\Psi}}{\partial \bar{\mathbf{E}}^0}. \tag{2.43}$$

The macroscopic electroelastic moduli are

$$\tilde{\mathcal{A}}^0_{ijkl} = \frac{\partial^2 \tilde{\Psi}}{\partial \bar{\mathbf{F}} \partial \bar{\mathbf{F}}}, \quad \tilde{\mathcal{G}}^0_{ijk} = \frac{\partial^2 \tilde{\Psi}}{\partial \bar{\mathbf{F}} \partial \bar{\mathbf{E}}^0} \quad \text{and} \quad \tilde{\mathcal{E}}^0_{ij} = \frac{\partial^2 \tilde{\Psi}}{\partial \bar{\mathbf{E}}^0 \partial \bar{\mathbf{E}}^0}. \tag{2.44}$$

Together with (2.12), the electroelastic moduli defined in equation (2.44) provide the coefficients for the polynomial equation (2.18), and, consequently, the onset of the macroscopic instabilities can be determined.

3. Examples

The energy-density function of an isotropic material can be expressed in terms of the invariants of the Cauchy–Green strain tensor $\mathbf{C} \equiv \mathbf{F}^{\mathrm{T}}\mathbf{F}$ and the nominal electric field $\mathbf{E}^0$ [43]. It is possible to express these invariants in the following form:

$$I_1 = \mathrm{Tr}\,\mathbf{C}, \quad I_2 = \tfrac{1}{2}(I_1^2 - \mathrm{Tr}(\mathbf{CC})), \quad I_3 = \det \mathbf{C}, \quad I_{4e} = \mathbf{E}^0 \cdot \mathbf{E}^0,$$
$$I_{5e} = \mathbf{E}^0 \cdot \mathbf{C}^{-1}\mathbf{E}^0 \quad \text{and} \quad I_{6e} = \mathbf{E}^0 \cdot \mathbf{C}^{-2}\mathbf{E}^0.$$

Accordingly, the energy-density function can be written as $\Psi(\mathbf{F}, \mathbf{E}^0) = \Psi(I_1, I_2, I_3, I_{4e}, I_{5e}, I_{6e})$. The expressions for the electroelastic moduli listed in equation (2.44) can be determined by application of the chain rule (appendix B).

As an example, we examine composites whose phase behaviours are characterized by a constitutive model of neo-Hookean soft dielectrics, namely

$$\Psi = \frac{\mu}{2}(I_1 - 3) - \frac{\epsilon}{2} I_{5e}, \tag{3.1}$$

where μ is the shear modulus and ϵ is the dielectric constant. For this choice of energy-density function, α in equation (2.23) is expressed as [44]

$$\alpha = \frac{\mu^{(f)} - \mu^{(m)}}{c^{(m)}\mu^{(f)} + c^{(f)}\mu^{(m)}} \frac{\bar{\mathbf{F}}\hat{\mathbf{N}} \cdot \bar{\mathbf{F}}\hat{\mathbf{M}}}{\bar{\mathbf{F}}\hat{\mathbf{M}} \cdot \bar{\mathbf{F}}\hat{\mathbf{M}}}. \tag{3.2}$$

Combining (2.22) with (2.21) and the constitutive law for each phase, namely,

$$\mathbf{D}^0 = \epsilon J \mathbf{F}^{-1}\mathbf{F}^{-\mathrm{T}}\mathbf{E}^0, \tag{3.3}$$

together with (2.23), (3.2) and noting that $\mathbf{F}^{(m)-\mathrm{T}}\hat{\mathbf{N}} = \mathbf{F}^{(f)-\mathrm{T}}\hat{\mathbf{N}} = \bar{\mathbf{F}}^{-\mathrm{T}}\hat{\mathbf{N}}$, we find that

$$\beta = \frac{\epsilon^{(f)} - \epsilon^{(m)}}{c^{(m)}\epsilon^{(f)} + c^{(f)}\epsilon^{(m)}} \frac{(\bar{\mathbf{F}}^{-\mathrm{T}}\bar{\mathbf{E}}^0) \cdot (\bar{\mathbf{F}}^{-\mathrm{T}}\hat{\mathbf{N}})}{(\bar{\mathbf{F}}^{-\mathrm{T}}\hat{\mathbf{N}}) \cdot (\bar{\mathbf{F}}^{-\mathrm{T}}\hat{\mathbf{N}})} + \alpha \bar{\mathbf{E}}^0 \cdot \hat{\mathbf{M}}. \tag{3.4}$$

The difference between the pressure terms in the two phases is

$$p^{(m)} - p^{(f)} = \frac{(\epsilon^{(f)} - \epsilon^{(m)})(\check{\epsilon}^2/\epsilon^{(m)}\epsilon^{(f)})((\bar{\mathbf{F}}^{-\mathrm{T}}\bar{\mathbf{E}}^0) \cdot (\bar{\mathbf{F}}^{-\mathrm{T}}\hat{\mathbf{N}}))^2 + \mu^{(m)} - \mu^{(f)}}{(\bar{\mathbf{F}}^{-\mathrm{T}}\hat{\mathbf{N}}) \cdot (\bar{\mathbf{F}}^{-\mathrm{T}}\hat{\mathbf{N}})}, \tag{3.5}$$

where $\check{\epsilon} = (c^{(m)}/\epsilon^{(m)} + c^{(f)}/\epsilon^{(f)})^{-1}$. Expression (3.5) reduces to the result obtained by deBotton [44] in the purely mechanical case. We note that (3.2), (3.4) and (3.5) provide an exact solution for the fields in each phase as functions of the average macroscopic deformation gradient $\bar{\mathbf{F}}$ and the nominal electric field $\bar{\mathbf{E}}^0$. These expressions for the fields can be used in the analysis to determine the onset of the microscopic instabilities.

Moreover, the total energy-density function of the composite is an exact expression obtained upon substitution of (3.2) and (3.4) into (2.42). Consequently, the electroelastic moduli in equation (2.44) for the composite are explicit expressions stemming from the solution of the homogenization problem. In turn, the onset of the macroscopic failure can be determined by finding a real root for characteristic equation (2.18).

We examine the case where, in the undeformed configuration, the applied electric field is aligned with one of the principal axes of the deformation gradient (figure 2), namely,

$$\bar{\mathbf{E}}^0 = E_2\bar{\mathbf{e}}_2 \quad \text{and} \quad \bar{\mathbf{F}} = \lambda\bar{\mathbf{e}}_1 \otimes \bar{\mathbf{e}}_1 + \lambda^{-1}\bar{\mathbf{e}}_2 \otimes \bar{\mathbf{e}}_2 + \bar{\mathbf{e}}_3 \otimes \bar{\mathbf{e}}_3. \tag{3.6}$$

However, in general, the layer directions are not aligned with the principal system and in terms of the lamination angle are $\hat{\mathbf{N}} = \sin\Theta\,\bar{\mathbf{e}}_1 + \cos\Theta\,\bar{\mathbf{e}}_2$ and $\hat{\mathbf{M}} = \cos\Theta\,\bar{\mathbf{e}}_1 - \sin\Theta\,\bar{\mathbf{e}}_2$. The corresponding expressions for the governing matrices of the microscopic instability analysis $\mathbf{Q}$ and $\mathbf{R}$ are rather complicated in this case. However, for the aligned case $\Theta = 0$, a significant simplification occurs, in particular the non-zero entries of $\mathbf{R}$ are

$$R_{12} = 1, \quad R_{21} = k_1^2\lambda^4\left(1 + \frac{E_2^2\epsilon}{\mu}\right), \quad R_{25} = -\frac{\mathrm{i}k_1E_2\lambda^3\epsilon}{\mu}, \quad R_{26} = \frac{\mathrm{i}k_1\lambda^2}{\mu},$$
$$R_{31} = R_{54} = -R_{45} = -\mathrm{i}k_1, \quad R_{52} = -\mathrm{i}k_1E_2\lambda, \quad R_{53} = -k_1^2E_2\lambda, \quad R_{62} = -\mathrm{i}k_1\mu\lambda^{-2},$$
$$R_{63} = -k_1^2\lambda^2(\mu + \epsilon E_2^2) \quad \text{and} \quad R_{64} = -k_1^2\epsilon E_2\lambda.$$

The corresponding non-zero entries of the matrix $\mathbf{Q}$ are

$$Q_{11} = Q_{23} = Q_{64} = -Q_{46} = 1, \quad Q_{32} = \mu\lambda^{-2}, \quad Q_{33} = \mathrm{i}k_1(p - \epsilon E_2^2\lambda^2), \quad Q_{34} = \epsilon E_2\lambda$$
$$Q_{41} = \mathrm{i}k_1(3\epsilon E_2^2\lambda^2 - \mu\lambda^{-2} - p), \quad Q_{45} = 2\epsilon E_2\lambda, \quad Q_{51} = -2\mathrm{i}k_1\epsilon E_2\lambda \quad \text{and} \quad Q_{55} = -\epsilon.$$

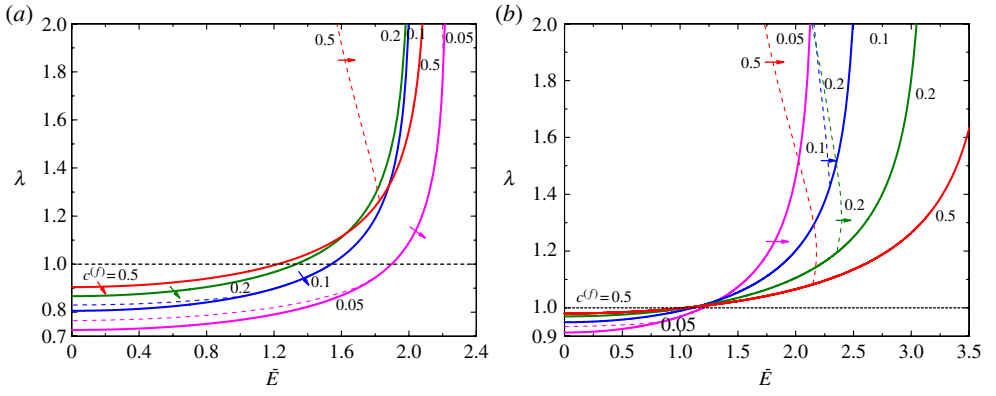

Figure 3. Critical stretch vs electric field for composites with $\Theta = 0$, $c^{(f)} = 0.05, 0.1, 0.2, 0.5$ and $k = t = 10$ (*a*), $k = t = 50$ (*b*). Continuous and dashed curves are for macroscopic and microscopic instabilities, respectively. (Online version in colour.)

Furthermore, the analytical expression for the onset of macroscopic instabilities takes a compact form when $\Theta = 0$. Namely, the critical stretch ratio is

$$\lambda_c = \left(1 - \frac{\breve{\mu}}{\bar{\mu}}\right)^{1/4} \left(1 - \bar{E}^2 \left(1 - \frac{\breve{\epsilon}}{\bar{\epsilon}}\right) \frac{\breve{\epsilon}}{\bar{\epsilon}}\right)^{-1/4}, \tag{3.7}$$

where $\bar{E} = E_2^0 \sqrt{\bar{\epsilon}/\bar{\mu}}$, $\bar{\epsilon} = c^{(m)}\epsilon^{(m)} + c^{(f)}\epsilon^{(f)}$, $\bar{\mu} = c^{(m)}\mu^{(m)} + c^{(f)}\mu^{(f)}$ and $\breve{\mu} = (c^{(m)}/\mu^{(m)} + c^{(f)}/\mu^{(f)})^{-1}$. Note that (3.7) is equivalent to the expression derived for similar setting in frame of the formulation employing the referential electrical displacement [40–42]. It is easy to see from (3.7) that the composites become macroscopically unstable if subjected to an electric excitation higher than

$$\bar{E}_c = \frac{\bar{\epsilon}}{\sqrt{(\bar{\epsilon} - \breve{\epsilon})\breve{\epsilon}}}. \tag{3.8}$$

An example of the bifurcation diagrams is shown in figure 3 for composites with $\Theta = 0$ as functions of the critical stretch ratio λ and the referential electric field $\bar{E}$. The curves separate stable domains from those in which instabilities may develop. The arrows indicate transitions from stable to unstable domains. The results are presented for $c^{(f)} = 0.05$, 0.1, 0.2 and 0.5, respectively. The stiffer to softer phase shear moduli ratio is $k = \mu^{(f)}/\mu^{(m)} = 10$ and the ratio between the dielectric constants is $t = \epsilon^{(f)}/\epsilon^{(m)} = 10$ in figure 3*a*.

For the macroscopic curves, we observe that an increase in the electric excitation extends the unstable domain, whereas the prestretch stabilizes the composite. This continues until the corresponding critical value of electric field (3.8) is achieved, beyond this value the composite becomes unstable regardless of the prestretch.

In a manner similar to the purely mechanical case, at low electric fields composites with low volume fractions of the stiffer phase ($c^{(f)} = 0.05$, 0.1) are more stable than those with moderate ones ($c^{(f)} = 0.2$, 0.5). However, when the electric field is increased, the curves intersect and instabilities in composites with lower $c^{(f)}$ may occur before those in composites with higher $c^{(f)}$. Specifically, at $\bar{E} = 1.95$ macroscopic instability occurs in a composite with $c^{(f)} = 0.1$ before it does in a composite with $c^{(f)} = 0.2$.

Interestingly, right before the intersection of the macroscopic curves, a curve corresponding to microscopic instability branches out from the curve for the macroscopic instability of the composite with higher $c^{(f)}$ such that practically the composite with higher volume fraction fails first, either at the macroscopic or at the microscopic level.

In composites with low volume fraction of the stiffer phase, there is a clear distinction between the onset of microscopic and macroscopic instabilities at low values of the applied electric field. In this limit, the microscopic instabilities that are associated with short waves appear long before the macroscopic ones. With the increase in the electric field, the curves for microscopic and

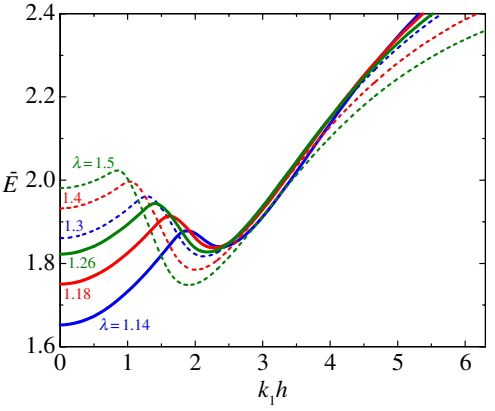

Figure 4. Critical electric field vs wave number for composite with $c^{(f)} = 0.5$ and $k = t = 10$. The continuous curves correspond to those loading parameters for which the first instability occurs at $k_1 h = 0$, whereas the dashed curves are for those parameters where the instability occurs at a finite wavelength. (Online version in colour.)

macroscopic instabilities near to the point where the macroscopic instabilities are the first to occur. However, the curves split again at high values of the electric excitation owing to the appearance of microscopic instabilities before the macroscopic ones.

At moderate volume fractions, the onset of the microscopic instability coincides with the macroscopic one (for example, $c^{(f)} = 0.2$). The curve of the microscopic instability branches from the curve of macroscopic instability only at large values of the electric field.

A similar behaviour is observed for composites with large volume fraction of the stiffer phase. However, the branching out of the curve for the microscopic instability occurs at lower values of the applied electric field. These branches of the instability curves reduce the stable domain and cut off the range of the prestretches at which the composite is stable. For example, for the composite with $c^{(f)} = 0.5$ subjected to $\bar{E} = 1.6$ the stable region of the stretch ratios is $1.1 < \lambda < 1.88$.

The dependence of the critical electric field on the dimensionless wave number $k_1 h$ for composite with volume fraction of the stiffer phase $c^{(f)} = 0.5$ is demonstrated in figure 4. The contrasts between the properties of the phases are $k = t = 10$. Along each curve, the prestretching is held constant. Before the branching out point of the curve for the microscopic instability in figure 3*a*, the minimal values of the electric field appear at $k_1 h \to 0$ corresponding to the macroscopic instabilities. An increase in the stretch ratio λ leads to a branching point at which minimum of the corresponding curve in figure 4 is attained at two points, one $k_1 h \to 0$ and the second at finite value of $k_1 h$. This happens because as we increase the prestretch, the critical electric field $\bar{E}$ at which the macroscopic instability occurs increases while the minimum at finite $k_1 h$ decreases. If we further increase the stretch ratio, the critical value of the wave number changes and the mode of instability shifts from macroscopic to a finite one.

The dependence of the critical stretch ratio on the electric field for composites with contrasts between the phases properties $k = t = 50$ is shown in figure 3*b*. The volume fractions of the stiffer phase are $c^{(f)} = 0.05$, 0.1, 0.2 and 0.5. As in the purely mechanical case [25,29], an increase in the contrast between the phases moduli results in earlier onsets of instabilities. Different from the case illustrated in figure 3*a* ($k = t = 10$), here the branching points of the curves corresponding to the microscopic instabilities appear even in composites with low volume fractions of the stiffer phase ($c^{(f)} = 0.1$) and at lower values of electric excitation, while the short-wave instabilities diminish. Thus, an increase in the contrasts between the phases properties restrains the short-wave instabilities (appearing at low values of $c^{(f)}$), and provokes earlier development of the microscopic instabilities that are characterized by finite wavelengths.

To complete the characterization of the composites stable domains, the projections of the bifurcation diagrams in coordinates of the electric field $\bar{E}$ and electric displacement

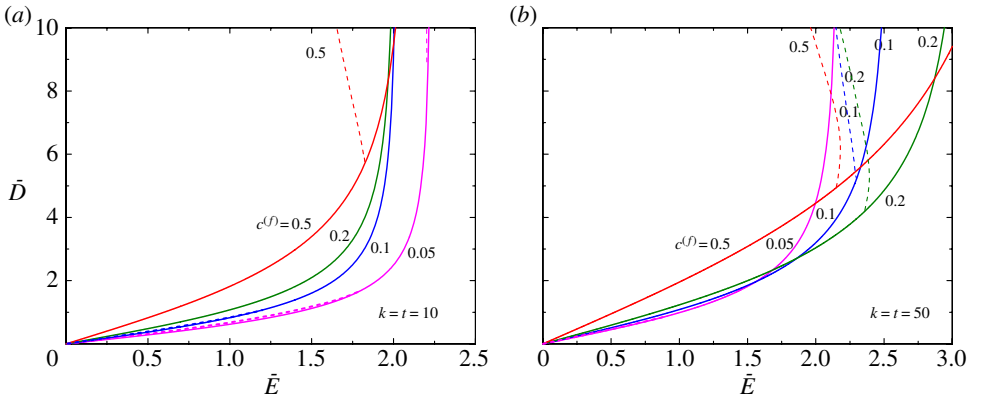

Figure 5. (*a*,*b*) Bifurcation diagrams as functions of the electric field $\bar{E}$ and electric displacement $\bar{D}$. Continuous and dashed curves represent the onset of macroscopic and microscopic instabilities, respectively. (Online version in colour.)

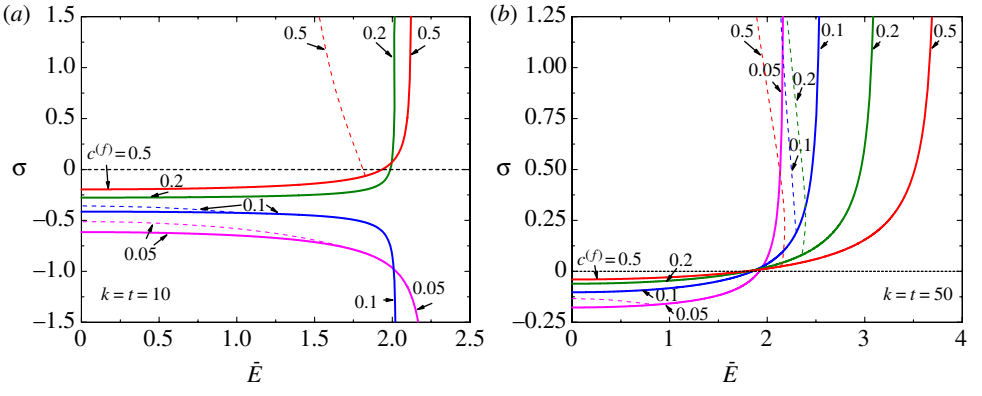

Figure 6. (*a*,*b*) Bifurcation diagrams as functions of longitudinal mean stress and referential electric field. Continuous and dashed curves represent the onset of macroscopic and microscopic instabilities, respectively. (Online version in colour.)

$\bar{D}=D_2^0/\sqrt{\mu^{(m)}\epsilon^{(m)}}$ are shown in figure 5*a*,*b*. The corresponding average referential electric displacement and electric field are related via

$$\bar{\mathbf{D}}^0=\bar{\epsilon}\bar{\mathbf{F}}^{-1}\bar{\mathbf{F}}^{-\mathrm{T}}\bar{\mathbf{E}}^0+(\check{\epsilon}-\bar{\epsilon})\bar{\mathbf{F}}^{-1}\bar{\mathbf{F}}^{-\mathrm{T}}\hat{\mathbf{N}}\frac{(\bar{\mathbf{F}}^{-\mathrm{T}}\bar{\mathbf{E}}^0)\cdot(\bar{\mathbf{F}}^{-\mathrm{T}}\hat{\mathbf{N}})}{(\bar{\mathbf{F}}^{-\mathrm{T}}\hat{\mathbf{N}})\cdot(\bar{\mathbf{F}}^{-\mathrm{T}}\hat{\mathbf{N}})}, \tag{3.9}$$

which reduces to the expression $D_2^0=\check{\epsilon}E_2^0\lambda^2$ reported in [42] for the aligned case $\Theta=0$.

To conclude the characterization of the stable domains, we also plot the bifurcation diagrams as functions of the applied electric field and the critical deviatoric mean stress along the layers. These are shown in figure 6 for the same contrasts between the phases properties, namely $k=t=10$ in (*a*) and $k=t=50$ in (*b*). Here this stress component is related to the stretch ratio and the electric field via $\bar{\sigma}^D/\bar{\mu}=((2-\bar{E}^2\check{\epsilon}/\bar{\mu})\lambda^2-1-\lambda^{-2})/3$. As anticipated on physical grounds, we observe that the critical macroscopic longitudinal stress is negative for relatively low applied electric fields. However, depending on the morphology, an increase in the electric field influences differently the critical mean stress. In particular, for composites with higher contrasts between the properties of the phases the critical stress increases (figure 6*b*), while for composites with lower contrasts the critical stress decreases when the volume fraction of the stiffer phase is low ($c^{(f)}=0.05$ and 0.1 in figure 6*a*) and increases when $c^{(f)}$ is high ($c^{(f)}=0.2$ and 0.5 in figure 6*a*).

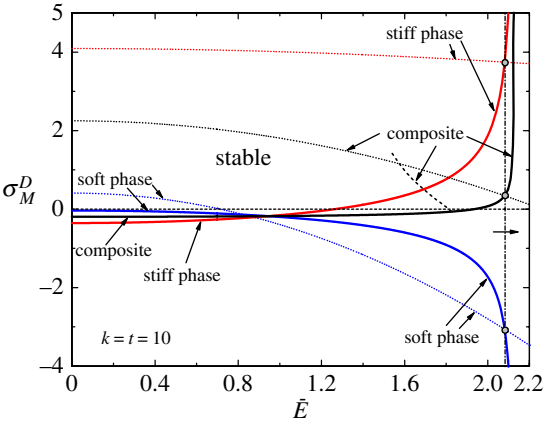

Figure 7. Stresses vs electric field in composites with $c^{(f)} = 0.5$. Dotted, continuous and dashed curves correspond to stresses along equilibrium path $\lambda = 2$, onset of macroscopic and microscopic instabilities, respectively. (Online version in colour.)

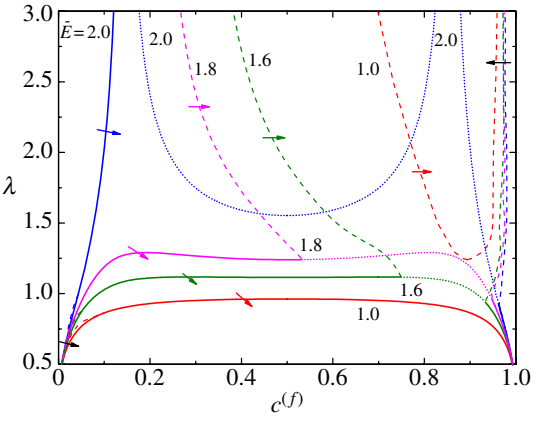

Figure 8. Critical stretch vs volume fraction for composites with $k = t = 10$. Continuous and dashed curves are for macroscopic and microscopic instabilities, respectively. Dotted curves separate unified unstable domains. (Online version in colour.)

Consider the evolution of the stresses in the phases of the material along the equilibrium path of a fixed prestretched configuration $\lambda = 2$. Shown in figure 7 are the variations of the longitudinal deviatoric stresses in the phases as functions of the applied electric field. The red and blue curves correspond to the stresses in the stiffer and softer phases, respectively, while the mean stresses are represented by the black curves (online version in colour). The dotted, continuous and dashed curves correspond to the stresses along the equilibrium path, onset of macroscopic and microscopic instabilities, respectively. Along the equilibrium path, the stresses in the phases are positive at the initial prestretch configuration where $\bar{E} = 0$, and an increase in the applied electric field leads to a decrease in the stresses in the phases. Because of the different electric fields in the phases, the stress in the soft phase decreases faster and becomes negative [20]. The difference in the deviatoric longitudinal stresses increases as the electric field is increased and the equilibrium curves intersect with the corresponding bifurcation curves.

The morphology significantly impacts the composite stability, restraining or promoting different instability modes. To highlight this effect, bifurcation diagrams are presented as functions of the critical stretch ratio and the volume fraction of the stiffer phase in figure 8. The failure surfaces are shown for composites with contrast ratios $k = t = 10$ subjected to different electrical excitations $\bar{E} = 1.0$, 1.6, 1.8 and 2.0.

We observe that for each unstable domain corresponding to a particular electric excitation, three subdomains can be distinguished. The first corresponds to the one where macroscopic instabilities ($k_1 h \to 0$) are identified. This macroscopically unstable domain lies beneath the continuous curves. The domain increases with the increase in the applied electric field. The second domain corresponds to a small zone at low volume fractions of the stiffer phase, between the dashed and the continuous curves. Here, instabilities associated with short waves ($k_1 h \to 2\pi$) appear. Different from the first domain, this one decreases with the increase in the electric excitation. So that the applied electric field restrains the short-wave instabilities and stimulates the long-waves instabilities. The above subdomains were observed for the purely mechanical case in [25,29]. The peculiar third domain was not revealed in the purely mechanical case. The characteristic scale of these instabilities is demonstrated in figure 4 and it appears to be $k_1 h \sim 2$. This domain is associated with high volume fraction of the stiffer phase and large prestretches. When the electric excitation increases the domain expands to include composites with moderate volume fractions at lower levels of the stretch ratio. As the first and third domains expand towards each other, the electric excitation increases, at some value of $\bar{E}$ they intersect. In the figure, we keep distinguishing between them with the aid of the dotted curves.

It was rigorously shown for the purely mechanical case that the long-waves instabilities can be estimated from the loss of strong ellipticity of the corresponding media [45]. Furthermore, the macroscopic instability is an upper bound for the microscopic instabilities. For the fully coupled electromechanical problem, we always observe this phenomenon during calculation of the numerical examples (e.g. figure 4). The numerical results for the aligned composites with some specific volume fractions are in agreement with the findings of [42]. In addition, we observe that for the media with moderate volume fractions of the stiffer phase, the macroscopic instability can be used as a good estimate for the material failure.

We consider next the influence of the lamination angle Θ on the onset of instabilities. Noting that at lamination angles different from $\Theta = 0$ and $\pi/2$, the microscopic instability analysis becomes rather complicated and for the non-aligned loading cases, we consider only the onset of *macroscopic* instabilities.

Bifurcation diagrams are presented in figure 9 as functions of the critical stretch ratio and the volume fraction of the stiffer phase for composites with different lamination angles $\Theta = 0, \pi/16, \pi/8$. The composites are subjected to electric excitation $\bar{E} = 1.0$ in figure 9*a* and $\bar{E} = 2.0$ in figure 9*b*. In a manner reminiscent of the purely mechanical case [29], the macroscopic failure surfaces are symmetric with respect to $c^{(f)} = 0.5$ and the composites are less stable in the range of moderate volume fraction of the stiffer phase. Composites with volume fractions near $c^{(f)} \sim 0$ and 1 become stable. This effect is intensified with an increase in the lamination angle, once again in a manner similar to the one observed in laminated composites under mechanical loads [46]. An increase in the electric excitation results in earlier onset of the macroscopic instability. The picture alters drastically when the value of the electric field is approaching $\bar{E}$ given in equation (3.8). In contrast to the findings in figure 9*a*, we observe in figure 9*b* that the composites with volume fractions of the stiffer phase in the vicinity of $c^{(f)} \sim 0.144$ and 0.856 become extremely unstable.

To highlight the transition of the composites behaviour as the intensity of the electric field approaches the critical value of the applied electric field, the bifurcation diagrams of composites with aligned layers ($\Theta = 0$) are presented in figure 10 for $\bar{E} = 1.9$, 1.925, 1.95, 1.975, 2.0 and 2.025. Thus, in contrast to the purely mechanical case where the least macroscopically stable morphology corresponds to $c^{(f)} = 0.5$, in the electromechanical case the volume fraction at which the least stable morphology is attained varies. Remarkably, the results of the numerical simulations hint that the dramatic change of the macroscopic curves can be associated with the unifying of the first and third unstable domains in figure 8. At this level of electrostatic excitation the media become unstable in a large range of $c^{(f)}$ (figure 8). We observe that at the macroscopic level the effect of the lamination angle varies from stabilizing the composite at low values of the electric field to the opposite effect at high electric excitations. However, this trend may be different when microscopic instabilities at shorter wavelengths are accounted for. Therefore, in the following examples, we consider composites with volume fraction of the stiffer phase

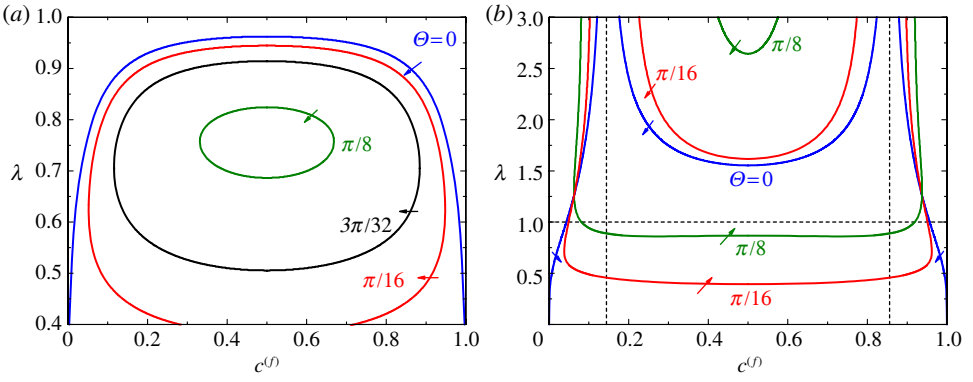

Figure 9. Critical stretch vs volume fractions for composites with $k = t = 10$. (*a*) $\bar{E} = 1.0$ and (*b*) $\bar{E} = 2.0$. (Online version in colour.)

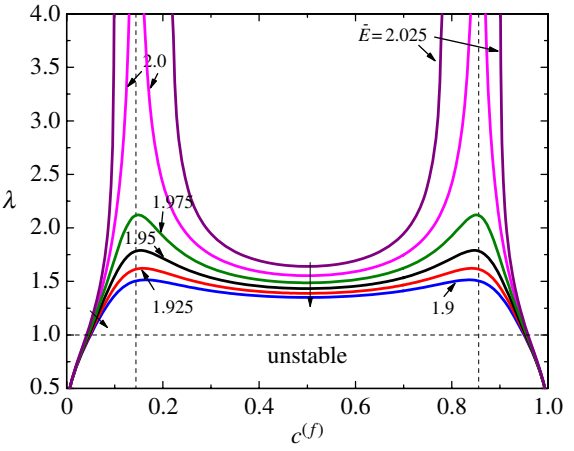

Figure 10. Critical stretch vs volume fraction for composites with $\Theta = 0$ and $k = t = 10$. (Online version in colour.)

$c^{(f)} = 0.2$ because the macroscopic failure mode dominates at this morphology even at relatively high electrostatic excitations. Shown in figure 11 are the bifurcation diagrams for composites with $c^{(f)} = 0.2$. The bifurcation diagrams are presented as functions of the critical stretch ratio λ and the referential electric field $\bar{E}$. The contrasts between the properties of the phases are $k = t = 10$. The lamination angles in the ranges $0 \leq \Theta \leq \pi/4$ and $\pi/4 < \Theta \leq \pi/2$ are presented in figure 11*a*,*b*, respectively. The continuous curves correspond to the macroscopic failure surfaces and the dashed curve in figure 11*a* represents the onset of the microscopic instability for the aligned case ($\Theta = 0$). The corresponding expression for the critical stretch ratio takes a compact form when $\Theta = \pi/2$

$$\lambda_c = \left(1 - \frac{\check{\mu}}{\bar{\mu}} - \bar{E}^2\left(1 - \frac{\check{\epsilon}}{\bar{\epsilon}}\right)\right)^{-1/4}. \tag{3.10}$$

In contrast to the aligned case ($\Theta = 0$), here an increase in the applied electric field stabilizes the media. It is easy to see from (3.10) that whenever the applied electric field exceeds the value

$$\bar{E}_c = \frac{\sqrt{(\bar{\mu} - \check{\mu})\bar{\epsilon}}}{\sqrt{(\bar{\epsilon} - \check{\epsilon})\bar{\mu}}}, \tag{3.11}$$

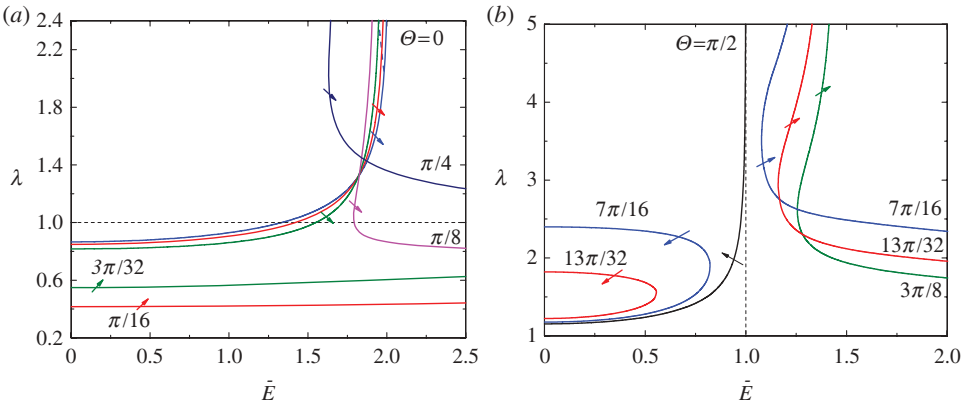

Figure 11. Critical stretch vs electric field for composites with $c^{(f)} = 0.2$ and $k = t = 10$. (*a*) small angles and (*b*) large angles. (Online version in colour.)

the composite becomes macroscopically stable. For the composite with identical shear to dielectric constants ratio of the phases $r^{(f)} = \mu^{(f)}/\epsilon^{(f)} = r^{(m)} = \mu^{(m)}/\epsilon^{(m)} = r$, this value of the electric field is $E_2^{0(c)} = \sqrt{r}$ which corresponds to $\bar{E}_c = 1$ (thin vertical dashed line in figure 11*b*).

In the pure mechanical case, the composites lose the stability only when the layers are compressed in the lamination direction. If the composite is laminated at an angle higher than a critical one, compressive loading will not lead to instabilities because the stretch in the layer direction switches from compression to tension as the layers rotate to an angle of more than $\pi/4$ in the deformed configuration [32]. However, in the coupled electromechanical case, when the electrostatic excitation is high enough even these composites may become unstable. For instance, the composites with $\Theta = \pi/8$ and $\Theta = \pi/4$ represented in figure 11 (pink and purple curves in online version) respectively. We also note that while in the purely mechanical case, the failure surfaces possess the property $\lambda(\Theta) = 1/\lambda(\Theta + \pi/2)$, the failure surfaces of the coupled problem do not.

In the limiting cases $\Theta = 0$ and $\Theta = \pi/2$, the role of the electric field varies from stimulating instabilities in the first case to stabilizing the composite in the latter. The behaviours of composites with intermediate lamination angles are associated with a transition between the limiting cases (from $\Theta = 0$ to $\Theta = \pi/2$) as far as the role of the electric field is concerned. Particularly, at some intermediate lamination angle, the role of the electric field switches. This is illustrated in figure 12 as a conclusive example for the composite with the previously considered phases properties and volume fractions. The diagrams show the dependence of the critical stretch ratio on the lamination angle. The applied electric excitations are $\bar{E} = 0.0$, 0.5, 1.0, 1.5, 1.8, 1.9 and 2.0, respectively. The bifurcation diagrams are symmetric with respect to 0 and $\pi/2$ and periodic in π. In agreement with the previous discussion, at low lamination angles the electric field promotes instabilities, whereas at lamination angles close to $\pi/2$ the applied electric field stabilizes the composites. Owing to this stabilizing effect, in composites with lamination angles close to $\pi/2$ instabilities may occur only under relatively low electric fields ($\bar{E} < 1$). We observe that at moderate levels of the electric field (e.g. $\bar{E} = 1.5$ and $\bar{E} = 1.8$), there are two disjoint unstable domains. The first contains the aligned composite ($\Theta = 0$) and the other includes composites with larger lamination angles at large critical stretch ratios. Composites with lamination angles between these two domains are macroscopically stable at these levels of excitations (e.g. composites with $0.11\pi < \Theta < 0.3\pi$ for $\bar{E} = 1.5$). With increase of the electric field, the unstable domains near and at a certain value of the electric field they unite (e.g. the transition from $\bar{E} = 1.8$ to $\bar{E} = 1.9$). Beyond this value of the electric field, the only stable morphology is the one with $\Theta = \pi/2$. Not surprisingly, the value of the lamination angle at which the domains unite corresponds to the morphology at which the influence of electric field switches.

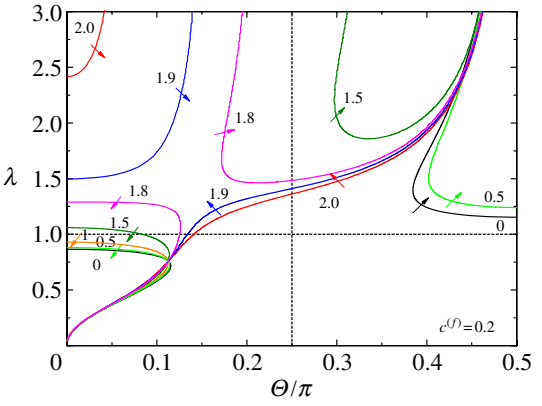

Figure 12. Critical stretch vs lamination angle for composite with $c^{(f)} = 0.2$ and $k = t = 10$. (Online version in colour.)

Note that for composites with isotropic phases in the cases $\Theta = n\pi, \pi/2 + n\pi$, where $n = 0, 1, 2\ldots$, the coefficients Γ_1, Γ_3, Γ_5 vanish in polynomial equation (2.18) and the condition for ellipticity loss can be written in terms of the bicubic polynomial

$$\Gamma_6\xi^6 + \Gamma_4\xi^4 + \Gamma_2\xi^2 + \Gamma_0 = 0. \tag{3.12}$$

Analogous results in terms of the nominal electric displacement instead of the referential electric field were reported for surface instabilities in a half-space isotropic dielectrics [39] and for long-wave instabilities in layered composites with isotropic phases and lamination angle $\Theta = 0$ [42].

4. Conclusion

A systematic study of multiscale instabilities in soft composite dielectrics was conducted in terms of physically relevant variables. First, a *general criterion* for the onset of instabilities associated with long waves was introduced. Second, a condition for the onset of microscopic instability was introduced for layered composites with *anisotropic* phases. Third, a closed form expression for energy-density function of this medium is deduced. These allowed to conclude that, depending on the morphology and the electromechanical loadings, laminated composites may fail in one of the three modes: (i) *long-wave* instabilities at moderate volume fractions of the stiffer phase; (ii) *interface instabilities* at low volume fractions of the stiffer phase and (iii) *instabilities at the microstructure characteristic length scale* at high volume fractions of the stiffer phase. An increase in the electric field suppresses the second mode of instabilities and promotes the first and third modes. At large enough electric excitation, the two domains that are dominated by these modes unite. At this stage, the composite becomes extremely unstable. This critical level of electric excitation can be detected by the more compact analysis of macroscopic instabilities. Whenever the macroscopic failure surfaces alter drastically as illustrated in figures 9 and 10, the critical excitation field is attained. Moreover, in the limiting cases of 0 and $\pi/2$ lamination angles explicit expressions for the onset of macroscopic instabilities were determined.

Finally, based on the analysis of the macroscopic instability domain, we find that at small lamination angles an increase in the electric field destabilizes the composite and vice versa at large lamination angles. The transition between these opposite effects occurs when the state of the stretch along the layers direction switches from compression to tension in the deformed configuration.

Funding statement. This work was supported by the US-Israel Binational Science Foundation (grant no. 2004146).

Appendix A. The components of the matrix **R**

The non-zero entries of **R** can be written as

$$R_{11} = k_1^2 b(\mathcal{G}_{122}(\mathcal{G}_{122} + \mathcal{G}_{221} - \mathcal{G}_{111}) - (\mathcal{A}_{1122} + \mathcal{A}_{1221} - \mathcal{A}_{1111})\mathcal{E}_{22}),$$

$$R_{12} = k_1^2 b(\mathcal{A}_{1121}\mathcal{E}_{22} - \mathcal{G}_{121}\mathcal{G}_{122}), \quad R_{13} = -\mathrm{i}k_1 b(\mathcal{G}_{111}\mathcal{E}_{22} + \mathcal{G}_{122}\mathcal{E}_{11}),$$

$$R_{14} = \mathrm{i}k_1 b(2\mathcal{G}_{122} - (\mathcal{G}_{112} + \mathcal{G}_{121})\mathcal{E}_{22}\mathcal{E}_{12}), \quad R_{15} = \mathrm{i}k_1 b\mathcal{E}_{22},$$

$$R_{16} = \mathrm{i}k_1 b(\mathcal{G}_{122}(\mathcal{G}_{112} + \mathcal{G}_{121} - \mathcal{G}_{222}) - (2\mathcal{A}_{1112} - \mathcal{A}_{1222})\mathcal{E}_{22})$$

$$R_{21} = bk_1^2\mathcal{E}_{22}^{-1}(\mathcal{G}_{122}^2 - \mathcal{A}_{1212}\mathcal{E}_{22})((\mathcal{A}_{1121} - 2\mathcal{A}_{2122})\mathcal{E}_{22} + \mathcal{G}_{222}(\mathcal{G}_{122} + \mathcal{G}_{221} - \mathcal{G}_{111})) - (\mathcal{A}_{1222} - \mathcal{E}_{22}^{-1}\mathcal{G}_{122}\mathcal{G}_{222})R_{11},$$

$$R_{22} = -k_1^2\{b(\mathcal{G}_{122}(\mathcal{A}_{1222}\mathcal{G}_{121} + \mathcal{A}_{1121}\mathcal{G}_{222}) - \mathcal{A}_{1121}\mathcal{A}_{1222}\mathcal{E}_{22} - \mathcal{A}_{1212}\mathcal{G}_{121}\mathcal{G}_{222}) + \mathcal{A}_{2121}\},$$

$$R_{23} = \mathrm{i}k_1\{\mathcal{G}_{121} - (\mathcal{A}_{1222}\mathcal{E}_{22}\mathcal{G}_{111} + (\mathcal{A}_{1212}\mathcal{G}_{222} - \mathcal{A}_{1222}\mathcal{G}_{122})\mathcal{E}_{11})b\},$$

$$R_{24} = -\mathrm{i}k_1\{(\mathcal{E}_{22}\mathcal{A}_{1222}(\mathcal{G}_{112} + \mathcal{G}_{121}) - 2\mathcal{E}_{12}(\mathcal{A}_{1222}\mathcal{G}_{122} + \mathcal{A}_{1212}\mathcal{G}_{222}) - \mathcal{G}_{122}(\mathcal{G}_{112} + \mathcal{G}_{121})\mathcal{G}_{222})b + \mathcal{G}_{122} + \mathcal{G}_{221}\}, \quad R_{25} = \mathrm{i}k_1 b(\mathcal{A}_{1222}\mathcal{E}_{22} - \mathcal{G}_{122}\mathcal{G}_{222}),$$

$$R_{26} = -\mathrm{i}k_1\mathcal{E}_{22}^{-1}\{((2\mathcal{A}_{1112} - \mathcal{A}_{1222})\mathcal{E}_{22} - \mathcal{G}_{122}(\mathcal{G}_{112} + \mathcal{G}_{121} - \mathcal{G}_{222}))(\mathcal{A}_{1222}\mathcal{E}_{22} - \mathcal{G}_{122}\mathcal{G}_{222})b - (\mathcal{A}_{1122} + \mathcal{A}_{1221} - \mathcal{A}_{2222})\mathcal{E}_{22} - (\mathcal{G}_{112} + \mathcal{G}_{121} - \mathcal{G}_{222})\mathcal{G}_{222}\},$$

$$R_{31} = k_1^2 b((\mathcal{A}_{1111} - \mathcal{A}_{1122} - \mathcal{A}_{1221})\mathcal{G}_{122} + \mathcal{A}_{1212}(\mathcal{G}_{122} + \mathcal{G}_{221} - \mathcal{G}_{111})),$$

$$R_{32} = k_1^2 b(\mathcal{A}_{1212}\mathcal{G}_{121} - \mathcal{A}_{1121}\mathcal{G}_{122}), \quad R_{33} = \mathrm{i}k_1 b(\mathcal{G}_{111}\mathcal{G}_{122} - \mathcal{A}_{1212}\mathcal{E}_{11}),$$

$$R_{34} = \mathrm{i}k_1 b((\mathcal{G}_{112} + \mathcal{G}_{121})\mathcal{G}_{122} - \mathcal{A}_{1212}\mathcal{E}_{12}), \quad R_{35} = -\mathrm{i}k_1 b\mathcal{G}_{122},$$

$$R_{36} = -\mathrm{i}k_1 b((\mathcal{A}_{1222} - 2\mathcal{A}_{1112})\mathcal{G}_{122} + \mathcal{A}_{1212}(\mathcal{G}_{112} + \mathcal{G}_{121} - \mathcal{G}_{222})) \quad R_{41} = -R_{54} = -\mathrm{i}k_1 \quad R_{66} = 1,$$

where $b = (\mathcal{A}_{1212}\mathcal{E}_{22} - \mathcal{G}_{122}^2)^{-1}$.

Appendix B. Derivatives of the electroelastic invariants

$$\frac{\partial I_1}{\partial F_{ij}} = 2F_{ij}, \quad \frac{\partial^2 I_1}{\partial F_{ij}\partial F_{kl}} = 2\delta_{ik}\delta_{jl}, \quad \frac{\partial I_{5e}}{\partial F_{pq}} = -2C_{qj}^{-1}E_j^0F_{ip}^{-1}E_i^0, \quad \frac{\partial I_{5e}}{\partial E_i^0} = 2C_{ij}^{-1}E_j^0$$

$$\frac{\partial^2 I_{5e}}{\partial F_{pq}\partial F_{kl}} = 2\left\{C_{qj}^{-1}E_j^0F_{ik}^{-1}E_i^0F_{lp}^{-1} + (C_{li}^{-1}E_i^0F_{qk}^{-1} + F_{ik}^{-1}E_i^0C_{lq}^{-1})F_{jp}^{-1}E_j^0\right\},$$

$$\frac{\partial^2 I_{5e}}{\partial F_{pq}\partial E_k^0} = -2(C_{qj}^{-1}E_j^0F_{kp}^{-1} + C_{qk}^{-1}E_j^0F_{jp}^{-1}), \quad \frac{\partial^2 I_{5e}}{\partial E_i^0\partial E_j^0} = 2C_{ij}^{-1}.$$

References

1. Pelrine R, Kornbluh R, Pei Q-B, Joseph J. 2000 High-speed electrically actuated elastomers with strain greater than 100%. *Science* **287**, 836–839. (doi:10.1126/science.287.5454.836)
2. Bar-Cohen Y. 2001 EAP history, current status, and infrastructure. In *Electroactive polymer (EAP) actuators as artificial muscles* (ed. Bar-Cohen Y), pp. 3–44. Bellingham, WA: SPIE Press.
3. Bhattacharya K, Li JY, Xiao Y. 2001 Electromechanical models for optimal design and effective behavior of electroactive polymers. In *Electroactive polymer (EAP) actuators as artificial muscles* (ed. Bar-Cohen Y), pp. 309–330. Washington, DC: SPIE Press.
4. Lacour S-P, Prahlad H, Pelrine R, Wagner S. 2004 Mechatronic system of dielectric elastomer actuators addressed by thin film photoconductors on plastic. *Sens. Actuators A Phys.* **111**, 288–292. (doi:10.1016/j.sna.2003.12.009)

5. Carpi F, DeRossi D. 2005 Improvement of electromechanical actuating performances of a silicone dielectric elastomer by dispersion of titanium dioxide powder. *IEEE Trans.* **12**, 835–843. (doi:10.1109/TDEI.2005.1511110)
6. Carpi F, Salaris C, De Rossi D. 2007 Folded dielectric elastomer actuators. *Smart Mater. Struct.* **16**, 300–305. (doi:10.1088/0964-1726/16/2/S15)
7. O'Halloran A, O'Malley F, McHugh P. 2008 A review on dielectric elastomer actuators, technology, applications, and challenges. *J. Appl. Phys.* **104**, 071101. (doi:10.1063/1.2981642)
8. Stoyanov H, Kollosche M, Risse S, McCarthy DN, Kofod G. 2011 Elastic block copolymer nanocomposites with controlled interfacial interactions for artificial muscles with direct voltage control. *Soft Matter* **7**, 194–202. (doi:10.1039/c0sm00715c)
9. Lu T, Huang J, Jordi C, Kovacs G, Huang R, Clarke DR, Suo Z. 2012 Dielectric elastomer actuators under equal-biaxial forces, uniaxial forces, and uniaxial constraint of stiff fibers. *Soft Matter* **8**, 6167–6173. (doi:10.1039/c2sm25692d)
10. Li W, Landis CM. 2012 Deformation and instabilities in dielectric elastomer composites. *Smart Mater. Struct.* **21**, 094006. (doi:10.1088/0964-1726/21/9/094006)
11. Thylander S, Menzel A, Ristinmaa M. 2012 An electromechanically coupled micro-sphere framework: application to the finite element analysis of electrostrictive polymers. *Smart Mater. Struct.* **21**, 094008. (doi:10.1088/0964-1726/21/9/094008)
12. Liu L. 2013 On energy formulations of electrostatics for continuum media. *J. Mech. Phys. Solids* **61**, 968–990. (doi:10.1016/j.jmps.2012.12.007)
13. Zhang QM, Li H, Poh M, Xia F, Cheng Z-Y, Xu H, Huang C. 2002 An all-organic composite actuator material with a high dielectric constant. *Nature* **419**, 284–289. (doi:10.1038/nature01021)
14. Huang C, Zhang QM, deBotton G, Bhattacharya K. 2004 All-organic dielectric-percolative three-component composite materials with high electromechanical response. *Appl. Phys. Lett.* **84**, 4391–4393. (doi:10.1063/1.1757632)
15. Ponte Castaneda P, Siboni MH. 2012 A finite-strain constitutive theory for electro-active polymer composites via homogenization. *Int. J. Nonlinear Mech.* **47**, 293–306. (doi:10.1016/j.ijnonlinmec.2011.06.012)
16. Gei M, Springhetti R, Bortot E. 2013 Performance of soft dielectric laminated composites. *Smart Mater. Struct.* **22**, 104014. (doi:10.1088/0964-1726/22/10/104014)
17. Javili A, Chatzigeorgiou G, Steinmann P. 2013 Computational homogenization in magneto-mechanics. *Int. J. Solids Struct.* **50**, 4197–4216. (doi:10.1016/j.ijsolstr.2013.08.024)
18. Huang C, Zhang QM. 2004 Enhanced dielectric and electromechanical responses in high dielectric constant all-polymer percolative composites. *Adv. Funct. Mater.* **14**, 501–506. (doi:10.1002/adfm.200305021)
19. deBotton G, Tevet-Deree L, Socolsky EA. 2007 Electroactive heterogeneous polymers: analysis and applications to laminated composites. *Mech. Adv. Mater. Struct.* **14**, 13–22. (doi:10.1080/15376490600864372)
20. Tian L, Tevet-Deree L, deBotton G, Bhattacharya K. 2012 Dielectric elastomer composites. *J. Mech. Phys. Solids* **60**, 181–198. (doi:10.1016/j.jmps.2011.08.005)
21. Rudykh S, Lewinstein A, Uner G, deBotton G. 2013 Analysis of microstructural induced enhancement of electromechanical coupling in soft dielectrics. *Appl. Phys. Lett.* **102**, 151905. (doi:10.1063/1.4801775)
22. Kolle M, Lethbridge A, Kreysing M, Baumberg JJ, Aizenberg J, Vukusic P. 2013 Bio-inspired band-gap tunable elastic optical multilayer fibers. *Adv. Mater.* **25**, 2239–2245. (doi:10.1002/adma.201203529)
23. Mockensturm EM, Goulbourne N. 2006 Dynamic response of dielectric elastomers. *Int. J. Nonlinear Mech.* **41**, 388–395. (doi:10.1016/j.ijnonlinmec.2005.08.007)
24. Rudykh S, Bhattacharya K, deBotton G. 2012 Snap-through actuation of thick-wall electroactive balloons. *Int. J. Nonlinear Mech.* **47**, 206–209. (doi:10.1016/j.ijnonlinmec.2011.05.006)
25. Li Y, Kaynia N, Rudykh S, Boyce MC. 2013 Wrinkling of interfacial layers in stratified composites. *Adv. Eng. Mater.* **15**, 921–926. (doi:10.1002/adem.201200387)
26. Rudykh S, Boyce MC. In press. Transforming wave propagation in layered media via instability-induced interfacial wrinkling. *Phys. Rev.*
27. Biot MA. 1965 *Mechanics of incremental deformations*. New York, NY: John Wiley and Sons.

28. Hill R, Hutchinson JW. 1975 Bifurcation phenomena in the plane tension test. *J. Mech. Phys. Solids* **23**, 239–264. (doi:10.1016/0022-5096(75)90027-7)
29. Triantafyllidis N, Maker BN. 1985 On the comparison between microscopic and macroscopic instability mechanisms in a class of fiber-reinforced composites. *J. Appl. Mech., Trans. ASME* **52**, 794–800. (doi:10.1115/1.3169148)
30. Fleck N. 1997 Compressive failure of fiber composites. *Adv. Appl. Mech.* **33**, 43–117. (doi:10.1016/S0065-2156(08)70385-5)
31. Bertoldi K, Boyce MC. 2008 Wave propagation and instabilities in monolithic and periodically structured elastomeric materials undergoing large deformations. *Phys. Rev. B* **78**, 184107. (doi:10.1103/PhysRevB.78.184107)
32. Rudykh S, deBotton G. 2012 Instabilities of hyperelastic fiber composites: micromechanical versus numerical analyses. *J. Elast.* **106**, 123–147. (doi:10.1007/s10659-011-9313-x)
33. Plante J-S, Dubowsky S. 2006 Large-scale failure modes of dielectric elastomer actuators. *Int. J. Solids Struct.* **43**, 7727–7751. (doi:10.1016/j.ijsolstr.2006.03.026)
34. De Tommasi D, Puglisi G, Saccomandi G, Zurlo G. 2010 Pull-in and wrinkling instabilities of electroactive dielectric actuators. *J. Phys. D Appl. Phys.* **43**, 325501. (doi:10.1088/0022-3727/43/32/325501)
35. Kofod G, Sommer-Larsen P, Kornbluh R, Pelrine R. 2003 Actuation response of polyacrylate dielectric elastomers. *J. Intel. Mater. Syst. Struct.* **14**, 787–793. (doi:10.1177/104538903039260)
36. Wang Q, Zhang L, Zhao X. 2011 Creasing to cratering instability in polymers under ultrahigh electric fields. *Phys. Rev. Lett.* **106**, 118301. (doi:10.1103/PhysRevLett.106.118301)
37. Liu L, Liu Y, Zhang Z, Li B, Leng J. 2010 Electromechanical stability of electro-active silicone filled with high permittivity particles undergoing large deformation. *Smart Mater. Struct.* **19**, 115025. (doi:10.1088/0964-1726/19/11/115025)
38. Molberg M, Crespy D, Rupper P, Nueesch F, Manson JAE, Loewe C, Opris DM. 2010 High breakdown field dielectric elastomer actuators using encapsulated polyaniline as high dielectric constant filler. *Adv. Funct. Mater.* **20**, 3280–3291. (doi:10.1002/adfm.201000486)
39. Dorfmann A, Ogden RW. 2010 Nonlinear electroelastostatics: Incremental equations and stability. *Int. J. Eng. Sci.* **48**, 1–14. (doi:10.1016/j.ijengsci.2008.06.005)
40. Rudykh S, deBotton G. 2011 Stability of anisotropic electroactive polymers with application to layered media. *Z. Angew. Math. Phys.* **62**, 1131–1142. (doi:10.1007/s00033-011-0136-1)
41. Rudykh S, Bertoldi K. 2013 Stability of anisotropic magnetorheological elastomers in finite deformations: a micromechanical approach. *J. Mech. Phys. Solids* **61**, 949–967. (doi:10.1016/j.jmps.2012.12.008)
42. Bertoldi K, Gei M. 2011 Instabilities in multilayered soft dielectrics. *J. Mech. Phys. Solids* **59**, 18–42. (doi:10.1016/j.jmps.2010.10.001)
43. Dorfmann A, Ogden RW. 2005 Nonlinear electroelasticity. *Acta Mech.* **174**, 167–183. (doi:10.1007/s00707-004-0202-2)
44. deBotton G. 2005 Transversely isotropic sequentially laminated composites in finite elasticity. *J. Mech. Phys. Solids* **53**, 1334–1361. (doi:10.1016/j.jmps.2005.01.006)
45. Geymonat G, Müller S, Triantafyllidis N. 1993 Homogenization of nonlinearly elastic materials, microscopic bifurcation and macroscopic loss of rank-one convexity. *Arch. Ration. Mech. Anal.* **122**, 231–290. (doi:10.1007/BF00380256)
46. Nestorovic MD, Triantafyllidis N. 2004 Onset of failure in finitely strained layered composites subjected to combined normal and shear loading. *J. Mech. Phys. Solids* **52**, 941–974. (doi:10.1016/j.jmps.2003.06.001)